IOP Publishing Journal of Physics B: Atomic, Molecular and Optical Physics
J. Phys. B: At. Mol. Opt. Phys. **57** (2024) 035001 (11pp) https://doi.org/10.1088/1361-6455/ad2182

# Statistical RTA simulations of atomic data for astrophysical opacity modeling in the context of kilonova emission

**H Carvajal Gallego[1], J-C Pain[2,3], M Godefroid[4], P Palmeri[1,*] and P Quinet[1,5]**

[1] Physique Atomique et Astrophysique, Université de Mons—UMONS, B-7000 Mons, Belgium
[2] CEA, DAM, DIF, F-91297 Arpajon, France
[3] Laboratoire Matière en Conditions Extrêmes, CEA, Université Paris-Saclay, F-91680 Bruyères-le-Châtel, France
[4] SQUARES, Université Libre de Bruxelles, B-1050 Bruxelles, Belgium
[5] IPNAS, Université de Liège, B-4000 Liège, Belgium

E-mail: patrick.palmeri@umons.ac.be

Received 14 November 2023, revised 29 December 2023
Accepted for publication 23 January 2024
Published 7 February 2024

**Abstract**

When considering some complex lanthanide ions characterized by a half-filled 4f subshell, the atomic structure Hamiltonian matrix sizes are so large that their diagonalization is challenging and therefore the atomic data of these ions are only used to compute the expansion opacity of a kilonova with difficulty. To avoid this problem, we propose a statistical simulation method to compute kilonova expansion opacities based on the resolved transition array (RTA) method of Bauche *et al* (1991 *Phys. Rev.* A **44** 5707). The atomic structure relativistic Hartree–Fock (HFR) method has been employed to compute the radial integrals necessary for our statistical RTA simulations where the atomic data are randomly drawn using their corresponding statistical distributions and to determine the exact expansion opacities where the atomic data are obtained by the diagonalization of the Hamiltonian matrix. The statistical RTA simulations carried out for two specific ions, i.e. Sm VIII and Eu VI, for which it is still possible to diagonalize the Hamiltonian matrix, reproduce well the expansion opacities computed using HFR atomic data. Based on this good agreements, the statistical RTA method was used to compute the expansion opacity of Dy VIII, which is determined through diagonalization with difficulty. The proposed statistical RTA simulation method allows the computation of reliable astrophysical expansion opacities which are of paramount importance for kilonova light curve modeling and spectral analysis.

Keywords: atomic data, atomic processes, plasmas, opacity, kilonovae

## 1. Introduction

For the past decade there has been a growing interest in elements heavier than iron following the detection of gravitational waves emanating from neutron star mergers and their corresponding electromagnetic signal in August 2017, identified as the GW170817 and AT2017gf0 events, respectively (Abbott 2017, Abbott *et al* 2017, Kasen *et al* 2017). These trans-iron heavy elements are abundantly produced through the nucleosynthesis r-process during the collision of neutron stars and are consequently found in the ejecta known as kilonova (Domoto *et al* 2022). Such elements are characterized by complex electronic configurations which result in a multitude of energy levels giving rise to a significant number of radiative transitions. Such elements absorb emitted light and the opacity affecting the kilonova spectrum is relatively high. Lanthanides ($Z = 57$–$71$), with their unfilled 4f subshell, are among the primary contributors to this opacity. Therefore, many investigations in recent years have been carried out to

* Author to whom any correspondence should be addressed.

evaluate the atomic properties and opacities of these elements. Notably, research has focussed on the first four ionization stages of lanthanides (typically encountered in kilonova conditions such as $t = 1$ day, $\rho = 10^{-13}$ g cm$^{-3}$ and temperatures below 20 000 K), specifically Nd II–IV (Gaigalas *et al* 2019), Er III (Gaigalas *et al* 2020), Pr-Gd II (Radžiūtė *et al* 2020), Tb-Yb II (Radžiūtė *et al* 2021), Ce II–IV (Carvajal Gallego *et al* 2021), Ce IV (Rynkun *et al* 2022) and all lanthanide ions across charge stages I to IV (Fontes *et al* 2020). The latter studies only concern lowly-charged lanthanide ions.

If the work is extended to higher temperatures (i.e. $T > 20\,000$ K), it is important to consider higher ionization degrees. They are of particular interest in the study of early-phase kilonovae (i.e. a few hours after the merger) and have been considered in recent works, among which are those we published for La V–X (Carvajal Gallego *et al* 2022a), Ce V–X (Carvajal Gallego *et al* 2022b), Pr–Nd–Pm V–X (Carvajal Gallego *et al* 2023), Sm V–X (Carvajal Gallego *et al* 2023a) and recently all the remaining lanthanides from the V to the VII charge state (Carvajal Gallego *et al* 2023b). All the calculations in the latter studies were performed with theoretical computational methods such as relativistic Hartree–Fock (HFR) (Cowan 1981) and multi-configuration Dirac Hartree–Fock (Froese Fischer *et al* 2019). To these studies must be added the calculations performed with Hebrew University Lawrence Livermore Atomic Code (HULLAC) (Bar-Shalom *et al* 2001) for Nd, Sm and Eu between the V and XI charge states and for elements ranging from La to Ra from the I to the XI charge states by Banerjee *et al* (2022, 2023).

When considering such complex ions, theoretical computational methods such as the HFR method implemented in Cowan's code (Cowan 1981) reach their computational limits. The dimensions of the Hamiltonian matrix are indeed so large that it becomes impractical to diagonalize it to obtain the eigenvalues and corresponding eigenvectors. For example, in the case of some lanthanide ions ranging between the VIII–X charge states, the eigenvalue equation is solved with difficulty since the Hamiltonian matrix size exceeds the computational limits of Cowan's code at our disposal, i.e. 2000 per $J$-parity symmetry block. Therefore, to calculate the atomic data and compute the opacities for these ions, which are crucial to model the kilonova light curve, the matrix dimension issue has to be overcome. To circumvent this bottleneck, it is worthwhile to test a statistical approach. The latter is based on a random-number method that is used to simulate in a realistic way the energies and intensities of the radiative lines of an array, making full use of the array properties, and is called the resolved transition array (RTA) method (Bauche *et al* 1991, 2015). To benefit from this method, the ion studied has to be a chaotic system. Indeed, for such many-electron atoms with sufficient basis-state mixing, i.e. quantum-chaotic systems, the probability distribution of the line strength can be well approximated as uniform (Fujii and Berengut 2020). Moreover, there is no limitation in using this approach, that is to say, it can handle as many configurations as necessary to describe the electronic structure of the element considered. In some of the aforementioned studies, the results from the HULLAC method can be obtained for charge states up to XI, unless the model representing the ion is restricted to a few configurations (such as in the Banerjee *et al* (2022, 2023) works). If the convergence of a model is tested by increasing the number of configurations (such as in the Deprince *et al* (2023) paper for U III), computational methods rapidly show their limits and the statistical approach could be a reliable alternative.

In the present work, we give an overview of the statistical formulae used to calculate atomic data with the RTA method. The latter is applied to Sm VIII and Eu VI ions for which atomic data are also calculated with HFR. An opacity comparison between the computational theoretical method and the RTA method is also presented for the latter ions to finally apply the statistical method to Dy VIII, a complex ion difficult to solve with Cowan's code.

## 2. Statistical RTA method

The statistical RTA method was originally developed by Bauche *et al* (1991) and fully described in Bauche *et al* (1991, 2015). In this method, the diagonalization of a large Hamiltonian matrix is avoided and only a set of radial wave equations is solved for each electronic configuration in order to determine all the radial integrals and parameters appearing in the compact formulae. In what follows, we will recall and focus on the main tools to obtain the energy levels, transition wavelengths and oscillator strengths needed for the expansion opacity computation.

### 2.1. Energy levels

$N_C$ energy levels, $E$, are drawn randomly for each electronic configuration $C$ considered in our model using their corresponding statistical distribution. The latter are approximated by a Gaussian, i.e. for a configuration $C$:

$$D_C(E) = \frac{N_C}{2\pi\sqrt{v_C}} \exp\left[-\frac{(E - E_{\rm av})^2}{2v_C}\right], \qquad (1)$$

where $E_{\rm av}$ is the average energy of the configuration $C$, a radial parameter (a linear combination of radial integrals) as defined in equation (8.9) in Cowan (1981) which can be determined by solving the set of radial wave equations for the electronic configuration $C$, here the pseudo relativistic Hartree–Fock equations (Cowan 1981), $v_C$ is the variance of the distribution which is computed from compact formulae tabulated in e.g. table 3.2 in Bauche *et al* (2015). The latter depends upon products of Slater and spin-orbit radial integrals obtained with the same method as for the radial parameter $E_{\rm av}$. The total number of levels $N_C$ of a configuration $C$ is given by the following compact formula (Bauche *et al* 2015) (in the approximation of a Gaussian distribution of magnetic quantum numbers

$M$ of a configuration $C$) depending on whether the configuration possesses an odd or an even number of electrons:

$$N_C = \frac{2g(C)}{[8\pi\, v_M(C)]^{1/2}} \begin{cases} \left[1 - \dfrac{1}{6v_M(C)}\right] & \text{odd} \\ \left[1 - \dfrac{1}{24v_M(C)}\right] & \text{even} \end{cases}, \tag{2}$$

where $g(C)$ is the configuration degeneracy (Cowan 1981) and $v_M(C)$ is the variance of the distribution of magnetic quantum number $M$ of configuration $C$ (Bauche *et al* 2015).

The distribution of levels as a function of their total momentum quantum number $J$, $N_C(J)$, is given by Bauche and Bauche-Arnoult (1987) (in the approximation of a Gaussian distribution, i.e. with $\alpha_4 = 3$):

$$N_C(J) = \frac{g(C)}{v_M(C)\,(8\pi\, v_M(C))^{1/2}}\,(2J+1)\exp\left[-\frac{(2J+1)^2}{8v_M(C)}\right]. \tag{3}$$

Note that $N_C = \sum_J N_C(J)$ and therefore the random draw of $N_C(J)$ energy levels can be done using the distribution $D_C(E)$ presented in equation (1) for each value of $J$. This is the procedure followed in this work in order to take into account the selection rules in the next subsection.

### 2.2. Transition wavelengths

For each electric dipole (E1) transition array $C_l - C_u$ between a lower configuration $C_l$ and an upper configuration $C_u$ of opposite parities, the wavelengths, $\lambda_{lu}$, of $L(C_l - C_u)$ transitions are calculated as follows:

$$\lambda_{lu} = \frac{1}{\sigma_{lu}} = \frac{hc}{(E_u - E_l)}, \tag{4}$$

where $\sigma_{lu}$ is the corresponding wavenumber and $E_l$ and $E_u$ are respectively the energy level of the lower configuration $C_l$ and the upper configuration $C_u$ drawn randomly that obey the E1 selection rules as described in the previous subsection.

The total number of E1 lines of a $C_l - C_u$ array, $L(C_l - C_u)$, can be estimated (Bauche *et al* 2015) by:

$$L(C_l - C_u) = \frac{3}{\sqrt{8\pi}} g(C_l)\, g(C_u)\, [v_M(C_l) + v_M(C_u)]^{-3/2} \times \left[1 - \frac{1}{v_M(C_l) + v_M(C_u)}\right]. \tag{5}$$

### 2.3. Oscillator strengths

The weighted oscillator strength, $g_l f_{lu}$, of each E1 line belonging to a $C_l - C_u$ array is determined by (Cowan 1981):

$$g_l f_{lu} = \left(3.0376 \times 10^{-6}\right)\, \sigma_{lu}\, S_{lu}, \tag{6}$$

where $g_l$ is the statistical weight of the lowest level $E_l$ of the transition, $\sigma_{lu} = E_u - E_l$ is expressed in $\mathrm{cm}^{-1}$ and is obtained randomly following the procedure described in the previous subsection, and the line strength $S_{lu}$ in a.u. is evaluated by $S_{lu} = \eta(C_l - C_u)a_{lu}^2$ through a random value of the line amplitude $a_{lu}$ (Bauche *et al* 1991) and a normalization factor $\eta(C_l - C_u)$ related to the total strength $S(C_l - C_u)$ of the $C_l - C_u$ array (Bauche *et al* 2015):

$$S(C_l - C_u) = S\left(n_1\ell_1^{N_1+1} n_2\ell_2^{N_2} n_3\ell_3^{N_3} - n_1\ell_1^{N_1} n_2\ell_2^{N_2+1} n_3\ell_3^{N_3}\right) \tag{7}$$

$$= 2\ell_> \binom{4\ell_1+1}{N_1}\binom{4\ell_2+1}{N_2} \times \binom{4\ell_3+2}{N_3} [P(n_1\ell_1, n_2\ell_2)]^2, \tag{8}$$

where $n_i\ell_i$ are open subshells, $\ell_>$ is the greater value between $\ell_1$ and $\ell_2$ and $P(n_1\ell_1, n_2\ell_2)$ is the E1 radial integral of $r$ between the central-field monoelectronic radial function $R_{n_1\ell_1}(r)/r$ and $R_{n_2\ell_2}(r)/r$ as determined by solving the radial equation.

As briefly mentioned previously, the transition amplitudes $a_{lu}$ are drawn randomly from a Gaussian distribution centered at zero a.u. with a variance, $v_a$, correlated with the line wavenumber, $\sigma_{lu}$, from the following equation (Bauche *et al* 1991):

$$\ln(v_a) = \alpha + \beta\,|\sigma - \sigma_{\mathrm{av}}|, \tag{9}$$

where $\sigma$ is the average of the range boundaries $\sigma = (\sigma_1 + \sigma_2)/2$ where the values of $\sigma_{lu}$ are distributed into consecutive ranges of equal widths on both sides of $\sigma_{\mathrm{av}}$, the average wavenumber of the $C_l - C_u$ array called unresolved transition array (UTA). Note that the UTA can be split into several peaks when the spin-orbit interaction becomes large. In this case, each peak is called a spin-orbit-split array (SOSA) and the same simulation has to be performed for each SOSA separately (Bauche *et al* 2015). The correlation parameters $\alpha$ and $\beta$ appearing in equation (9) can be determined *a posteriori* through a fitting procedure, or *ab initio,* through the following equations (Bauche *et al* 1991). The solution of the following implicit equation provides the value of $\beta$:

$$\left(X^2 + 1 - \frac{v_w}{v_{un}}\right)\exp\left(\frac{X^2}{2}\right)\mathrm{erfc}\left(\frac{X}{\sqrt{2}}\right) = X\sqrt{\frac{2}{\pi}}, \tag{10}$$

where $X = -\beta\sqrt{v_{un}}$, while the value of $\alpha$ is deduced from that of $X$ and from the average strength of the $C_l - C_u$ array, $S_{\mathrm{av}}(C_l - C_u)$, as follows:

$$\alpha = \ln[S_{\mathrm{av}}(C_l - C_u)] + \ln\left(X^2 + 1 - \frac{v_w}{v_{un}}\right) - \ln(X) + \frac{1}{2}\ln\left(\frac{\pi}{2}\right), \tag{11}$$

where $S_{\mathrm{av}}(C_l - C_u) = S(C_l - C_u)/L(C_l - C_u)$.

For equations (10) and (11), $v_{un}$ and $v_w$ are respectively the unweighted and weighted variances of the line wavenumber $\sigma_{lu}$ by the corresponding line strength $S_{lu}$. They can be evaluated by compact formulae for a $C_l - C_u$ UTA (Moszkowski 1962, Bauche-Arnoult *et al* 1979, 1982, Karazija and Rudzikaitė 1988, Karazija 1991).

### 2.4. A posteriori calculations

The *ab initio* statistical RTA atomic parameters and opacities will be tested through comparisons with HFR calculations and *a posteriori* statistical RTA calculations. Aside from the correlation parameters $\alpha$ and $\beta$ mentioned in the previous subsection, the latter essentially differs from the former in the sense that all the parameters of the different distributions are directly determined from the atomic data obtained after diagonalization of the Hamiltonian matrix using, e.g. the following formulae for the mean, $Q_{\rm av}$, and the variance, $v(Q)$, of a quantity $Q$ obtained through diagonalization:

$$Q_{\rm av} = \frac{\sum_i Q_i w_i}{\sum_i w_i}, \tag{12}$$

$$v(Q) = \frac{\sum_i (Q_i - Q_{\rm av})^2 w_i}{\sum_i w_i}, \tag{13}$$

where $Q_i$ can be the energy level $E_i$ belonging to a configuration $C$ or the wavenumber $\sigma_{lu}$ of a transition belonging to a $C_l - C_u$ array, $w_i$ is the weight that can be equal to 1 for unweighted moments or equal to the corresponding level degeneracy $g_i$ of a level $E_i$ belonging to a configuration $C$ or equal to the corresponding line strength $S_{lu}$ of a transition belonging to a $C_l - C_u$ array for weighted moments.

## 3. Calculation of astrophysical opacities

### 3.1. Expansion opacities

In order to compute these opacities, we used exactly the same procedure as the one employed in all our aforementioned papers (such as Carvajal Gallego *et al* (2021, 2022a, 2022b, 2023, 2023a, 2023b)). As a reminder, in a dynamic environment that expands rapidly, such as the one observed in the ejecta from neutron star mergers, the bound-bound transitions can be evaluated using the expansion formalism (Karp *et al* 1977, Eastman and Pinto 1993, Kasen *et al* 2006) according to which the contributions of a large number of lines to the monochromatic opacity are approximated by a discretization involving the summation of lines falling within a spectral width, while the radiative transfer is considered by the Sobolev (1960) approximation. The bound-bound opacity is calculated using

$$\kappa^{\rm bb}(\lambda) = \frac{1}{\rho c t} \sum_{lu} \frac{\lambda_{lu}}{\Delta\lambda} \left(1 - e^{-\tau_{lu}}\right), \tag{14}$$

where $\lambda$ (in Å) is the central wavelength within the region of width $\Delta\lambda$, $\lambda_{lu}$ are the wavelengths of the lines appearing in this range, $\tau_{lu}$ are the corresponding optical depths, $c$ (in cm/s) is the speed of light, $\rho$ (in g/cm$^3$) is the density of the ejected gas and $t$ (in s) is the elapsed time since ejection.

The optical depth can be expressed using the Sobolev (1960) formula:

$$\tau_{lu} = \frac{\pi e^2}{m_e c} f_{lu} n_l t \lambda_{lu}, \tag{15}$$

where $e$ (in C) is the elementary charge, $m_e$ (in g) is the electron mass, $f_{lu}$ (dimensionless) is the oscillator strength, and $n_l$ (in cm$^{-3}$) is the density of the lower level $E_l$ of the transition.

Let us also recall that, in this formalism, local thermodynamic equilibrium is assumed so that $n_l$ can be expressed using the Boltzmann distribution

$$n_l = \frac{g_l}{U(T)} n {\rm e}^{-E_l/k_B T}, \tag{16}$$

where $k_B$ is the Boltzmann constant (in cm$^{-1}$ K$^{-1}$), $T$ (in K) is the temperature, $g_l, E_l$ (in cm$^{-1}$) are respectively the statistical weight and the energy of the lower level of the transition, $n$ is the ionic density and $U(T)$ is the partition function defined as

$$U(T) = \sum_i g_i {\rm e}^{-E_i/kT}. \tag{17}$$

We can then write the optical depth as

$$\tau_{lu} = \frac{\pi {\rm e}^2}{m_e c} \frac{n \lambda_{lu} t}{U(T)} g_l f_{lu} {\rm e}^{-E_l/k_B T}. \tag{18}$$

The following subsections concern two lanthanide ions, namely Sm VIII and Eu VI, for which the atomic data are calculated by the HFR method with full matrix diagonalization and by the statistical RTA method. The goal is to check the reliability of the opacity computed with the statistical atomic data and reproduce a similar opacity to the one calculated with the HFR atomic data. In the last subsection, the statistical approach is applied to a moderately-charged lanthanide which is impossible to perform through diagonalization using the HFR method, namely Dy VIII.

### 3.2. Sm VIII and Eu VI

In Sm VIII, we have included the following six configurations in our full HFR calculation of the atomic data: $5p^4 4f^3$, $5p^3 4f^3 6p$, $5p^5 4f^2$ for the odd- and $5p^3 4f^3 5d$, $5p^3 4f^3 6s$, $5p^3 4f^3 7s$ for the even-parity. There are six E1 transition arrays since the electric dipole transition operator is monoelectronic. The $5p^5 4f^2$ configuration does not participate in any E1 transition array and is only included for configuration interaction (CI) purposes. Therefore, this configuration was not considered in our statistical RTA simulations, neither *a posteriori,* nor *ab initio*.

Regarding Eu VI, we have chosen to consider six configurations, namely $5p^6 4f^4$, $5p^5 4f^4 6p$, $5p^5 4f^5$ for the even- and $5p^5 4f^4 5d$, $5p^5 4f^4 6s$, $5p^5 4f^4 7s$ for the odd-parity, both in our full HFR calculation and in our *a posteriori* and *ab initio* statistical RTA simulations. Here, there are seven E1 transition arrays.

In these *a posteriori* statistical RTA simulations, we performed a statistical random draw considering both UTA and SOSA arrays, where the latter can be seen as a model that provides a higher resolution of the atomic spectrum or a better wavelength distribution of the oscillator strengths as a UTA can be split into several SOSA peaks. Therefore, one would expect that the opacity simulated by SOSA arrays would better

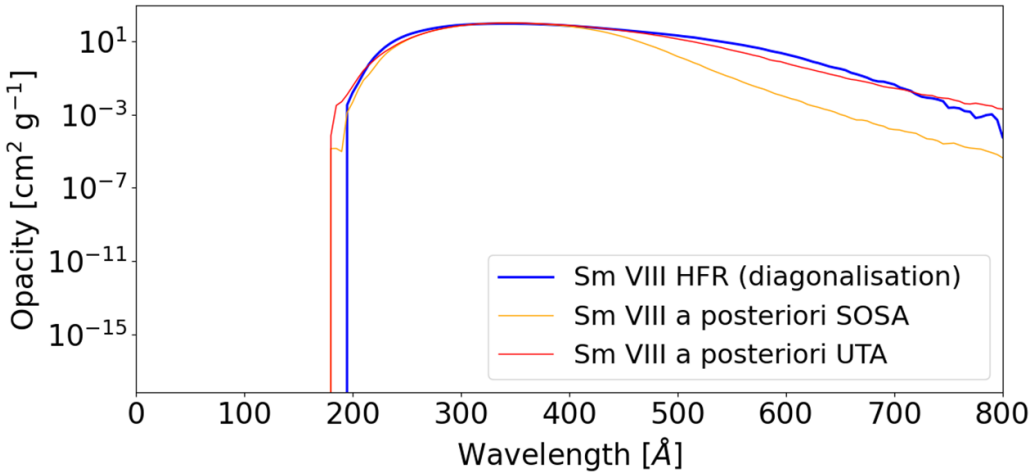


**Figure 1.** Expansion opacities computed in Sm VIII with $\rho = 10^{-10}$ g cm$^{-3}$, $t = 0.1$ day and $T = 50\,000$ K for the $5p^4 4f^3 - 5p^3 4f^3 5d$ array using the atomic data computed with the HFR method (blue curve), simulated with the *a posteriori* statistical RTA method considering SOSAs (orange curve) and considering a UTA (red curve).

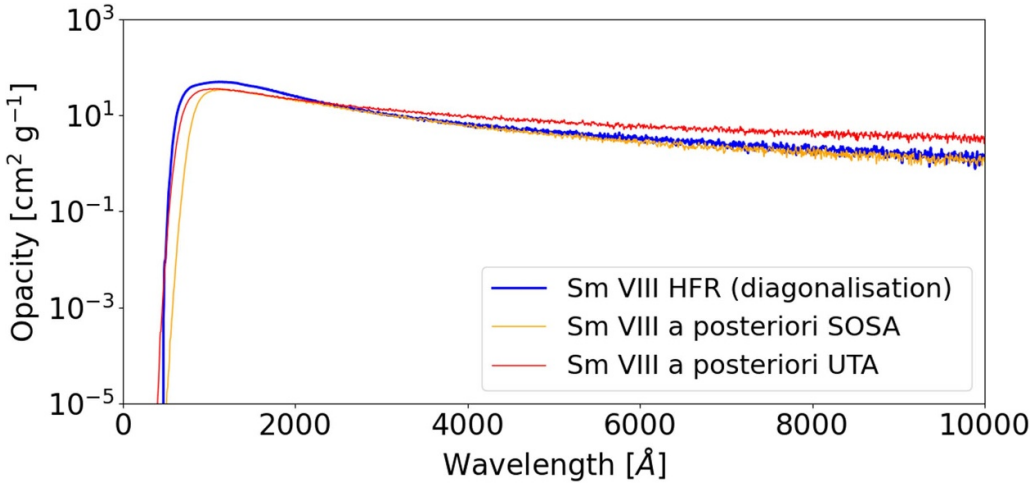


**Figure 2.** Expansion opacities computed in Sm VIII with $\rho = 10^{-10}$ g cm$^{-3}$, $t = 0.1$ day and $T = 50\,000$ K for the $5p^3 4f^3 6s - 5p^3 4f^3 6p$ array using the atomic data computed with the HFR method (blue curve), simulated with the *a posteriori* statistical RTA method considering SOSAs (orange curve) and considering a UTA (red curve).

reproduce the one obtained using the actual HFR atomic data. In fact, this is not always the case. For instance, in figure 1, we compare the use of both types of arrays along with a full HFR calculation for a specific array in Sm VIII, i.e. $5p^4 4f^3 - 5p^3 4f^3 5d$. It can be noticed that the UTA simulation reproduces better the HFR opacity than the one using SOSA arrays. A converse situation can be seen in figure 2 where the contribution of the array $5p^3 4f^3 6s - 5p^3 4f^3 6p$ in Sm VIII is shown. As a consequence, we have chosen for simplicity reasons, e.g. fewer statistical distributions are needed (Bauche *et al* 2015), to use UTAs in all our *ab initio* statistical RTA simulations.

In tables 1 and 2, we summarize the energy level distribution parameters, i.e. the average energy, $E_{\rm av}$, the standard deviation, $\sqrt{v_C}$, and the number of levels, $N_C$, for each configuration as considered in both the *a posteriori* and the *ab initio* RTA simulations for both ions, Sm VIII and Eu VI.

From these tables, it can be noticed that the results for the standard deviation and the number of levels are very similar. The total number of levels for all the configurations considered in all the E1 transition arrays for Sm VIII and Eu VI calculated *a posteriori* are respectively 15 498 and 13 065 whereas the *ab initio* values are 16 031 and 13 451. One has to stress that equation (2) (as well as equations (3) and (5) is an approximation and as explicitly written in Bauche *et al* (2015): '... no exact formula for the total number of the levels of a configuration is yet known, except in very simple cases like the $n\ell^2$ configurations, where it is equal to $(4\ell + 1)$, due to Pauli's principle.' Although the number of levels of a configuration and the number of lines can be exactly evaluated via standard atomic structure codes, statistical formulae (equations (2), (3) and (5)) are used for consistency with the *ab initio* statistical RTA method. Moreover, for Sm VIII, when the $5p^5 4f^2$ configuration is considered in the full HFR calculation (with CI), the total number of levels is 15 567. This configuration adds 69 levels contributing to the CI. We do not include the latter configuration in table 1 as it is not considered in

**Table 1.** Parameters of the statistical distribution of energy levels, $D_C(E)$, i.e. average energy, $E_{av}$, standard deviation, $\sqrt{v_C}$, and total number of levels, $N_C$, for each configuration in Sm VIII as considered in both statistical RTA calculations, namely *a posteriori* and *ab initio*.

| | | $\sqrt{v_C}$ (cm$^{-1}$) | | $N_C$ | |
|---|---|---|---|---|---|
| Configuration | $E_{av}$[a] (cm$^{-1}$) | *A posteriori*[b] | *Ab initio*[c] | *A posteriori*[d] | *Ab initio*[e] |
| $5p^4 4f^3$ | 78 888 | 38 958 | 40 705 | 589 | 620 |
| $5p^3 4f^3 5d$ | 357 248 | 50 678 | 53 416 | 7264 | 7494 |
| $5p^3 4f^3 6s$ | 484 513 | 42 286 | 44 007 | 1549 | 1603 |
| $5p^3 4f^3 7s$ | 704 571 | 42 446 | 44 125 | 1549 | 1603 |
| $5p^3 4f^3 6p$ | 556 742 | 43 581 | 45 289 | 4547 | 4711 |

[a] HFR radial parameter (see section 2.1).
[b] See section 2.4 and equation (13).
[c] Computed using HFR radial integrals and the compact formulae tabulated in Bauche *et al* (2015) (see section 2.1).
[d] See section 2.4.
[e] Computed using equation (2) (see section 2.1).

**Table 2.** Parameters of the statistical distribution of energy levels, $D_C(E)$, i.e. average energy, $E_{av}$, standard deviation, $\sqrt{v_C}$, and total number of levels, $N_C$, for each configuration in Eu VI as considered in both statistical RTA calculations, namely *a posteriori* and *ab initio*.

| | | $\sqrt{v_C}$ (cm$^{-1}$) | | $N_C$ | |
|---|---|---|---|---|---|
| Configuration | $E^a_{av}$ (cm$^{-1}$) | *A posteriori*[b] | *Ab initio*[c] | *A posteriori*[d] | *Ab initio*[e] |
| $5p^6 4f^4$ | 54 196 | 33 144 | 31 815 | 107 | 109 |
| $5p^5 4f^4 5d$ | 311 979 | 43 820 | 45 703 | 5756 | 5930 |
| $5p^5 4f^4 6s$ | 394 701 | 39 558 | 40 133 | 1222 | 1266 |
| $5p^5 4f^4 7s$ | 559 456 | 39 664 | 40 214 | 1222 | 1266 |
| $5p^5 4f^5$ | 148 108 | 40 991 | 42 095 | 1168 | 1199 |
| $5p^5 4f^4 6p$ | 454 489 | 39 904 | 40 792 | 3592 | 3681 |

[a] HFR radial parameter (see section 2.1).
[b] See section 2.4 and equation (13).
[c] Computed using HFR radial integrals and the compact formulae tabulated in Bauche *et al* (2015) (see section 2.1).
[d] See section 2.4.
[e] Computed using equation (2) (see section 2.1).

**Table 3.** Comparison between *a posteriori* and *ab initio* statistical RTA values for the number of lines, $L(C_l - C_u)$ and the total strength, $S(C_l - C_u)$), for each $C_l - C_u$ array in Sm VIII. The *ab initio* values of the corresponding unweighted, $\sqrt{v_{un}}$, and weighted, $\sqrt{v_w}$, standard deviations of the wavenumber distribution are also reported.

| | $L(C_l - C_u)$ | | $S(C_l - C_u)$ [a.u.] | | | |
|---|---|---|---|---|---|---|
| $C_l - C_u$ array | *A posteriori*[a] | *Ab initio*[b] | *A posteriori*[a] | *Ab initio*[c] | $\sqrt{v_{un}}^d$ (cm$^{-1}$) | $\sqrt{v_w}^d$ (cm$^{-1}$) |
| $5p^4 4f^3 - 5p^3 4f^3 5d$ | 1317 060 | 1639 731 | 31 296 | 62 388 | 57 898 | 24 224 |
| $5p^4 4f^3 - 5p^3 4f^3 6s$ | 228 243 | 367 067 | 2820 | 2807 | 52 599 | 25 493 |
| $5p^4 4f^3 - 5p^3 4f^3 7s$ | 253 897 | 367 067 | 333 | 332 | 52 723 | 26 714 |
| $5p^3 4f^3 6p - 5p^3 4f^3 5d$ | 8405 714 | 12 371 727 | 30 229 | 60 311 | 58 552 | 21 807 |
| $5p^3 4f^3 6p - 5p^3 4f^3 6s$ | 1656 733 | 2757 175 | 92 920 | 92 679 | 32 533 | 9054 |
| $5p^3 4f^3 6p - 5p^3 4f^3 7s$ | 1610 655 | 2757 175 | 23 032 | 22 970 | 52 134 | 9161 |

[a] Determined by diagonalization of the Hamiltonian (see section 2.4).
[b] Calculated using equation (5) (see section 2.2).
[c] Calculated using equation (8) (see section 2.3).
[d] Evaluated using the compact formulae of Bauche-Arnoult *et al* (1979, 1982)(see section 2.3).

the E1 transition arrays in the *a posteriori* statistical RTA simulation.

In tables 3 and 4, a comparison between *a posteriori* and *ab initio* statistical RTA values is presented for the number of lines, $L(C_l - C_u)$ and the total strength, $S(C_l - C_u)$), for each $C_l - C_u$ array in Sm VIII and Eu VI, respectively. The *ab initio* values of the corresponding unweighted, $\sqrt{v_{un}}$, and weighted, $\sqrt{v_w}$, standard deviations of the wavenumber distribution are also reported.

One can see that the number of lines calculated *ab initio* using equation (5) are systematically higher because there is no oscillator strength threshold, while in the *a posteriori* calculations based on the HFR atomic data we only consider lines with a $\log(gf) > -5$. The total number of lines are

**Table 4.** Comparison between *a posteriori* and *ab initio* statistical RTA values for the number of lines, $L(C_l - C_u)$ and the total strength, $S(C_l - C_u)$), for each $C_l - C_u$ array in Eu VI. The *ab initio* values of the corresponding unweighted, $\sqrt{v_{un}}$, and weighted, $\sqrt{v_w}$, standard deviations of the wavenumber distribution are also reported.

| | $L(C_l - C_u)$ | | $S(C_l - C_u)$ (a.u.) | | | |
|---|---|---|---|---|---|---|
| $C_l - C_u$ array | *A posteriori*[a] | *Ab initio*[b] | *A posteriori*[a] | *Ab initio*[c] | $\sqrt{v_{un}}^d$ ($cm^{-1}$) | $\sqrt{v_w}^d$ ($cm^{-1}$) |
| $5p^64f^4 - 5p^54f^45d$ | 171 563 | 218 988 | 9041 | 18 030 | 53 628 | 19 657 |
| $5p^64f^4 - 5p^54f^46s$ | 38 098 | 48 569 | 851 | 849 | 51 726 | 23 181 |
| $5p^64f^4 - 5p^54f^47s$ | 34 017 | 48 569 | 106 | 106 | 51 808 | 23 473 |
| $5p^54f^5 - 5p^54f^45d$ | 1640 627 | 2324 253 | 7783 | 23 291 | 51 714 | 18 690 |
| $5p^54f^46p - 5p^54f^45d$ | 4735 887 | 7210 500 | 33 620 | 33 537 | 45 001 | 14 872 |
| $5p^54f^46p - 5p^54f^46s$ | 900 390 | 1589 407 | 91 797 | 91 553 | 31 610 | 6248 |
| $5p^54f^46p - 5p^54f^47s$ | 857 607 | 1589 407 | 25 853 | 25 791 | 29 170 | 6392 |

[a] Determined by diagonalization of the Hamiltonian (see section 2.4).
[b] Calculated using equation (5) (see section 2.2).
[c] Calculated using equation (8) (see section 2.3).
[d] Evaluated using the compact formulae of Bauche-Arnoult *et al* (1979, 1982) (see section 2.3).

**Table 5.** Comparison between *a posteriori* and *ab initio* statistical RTA values of the average wavenumber, $\sigma_{av}$, and the correlation parameters $\alpha$ and $\beta$ for each $C_l - C_u$ array in Sm VIII.

| | $\sigma_{av}$ ($cm^{-1}$) | | $\alpha$ | | $\beta$ [cm] | |
|---|---|---|---|---|---|---|
| $C_l - C_u$ array | *A posteriori*[a] | *Ab initio*[b] | *A posteriori*[c] | *Ab initio*[d] | *A posteriori*[c] | *Ab initio*[e] |
| $5p^44f^3 - 5p^34f^35d$ | 324 611 | 329 727 | −4.60 | −1.94 | $-8.00 \times 10^{-5}$ | $-4.65 \times 10^{-5}$ |
| $5p^44f^3 - 5p^34f^36s$ | 390 379 | 410 223 | −1.92 | −3.73 | $-5.00 \times 10^{-5}$ | $-4.06 \times 10^{-5}$ |
| | 437 841 | | −2.37 | | $-4.00 \times 10^{-5}$ | |
| $5p^44f^3 - 5p^34f^37s$ | 608 898 | 628 642 | −5.85 | −5.92 | $-8.00 \times 10^{-5}$ | $-3.75 \times 10^{-5}$ |
| | 658 567 | | −5.95 | | $-1.00 \times 10^{-4}$ | |
| $5p^34f^36p - 5p^34f^35d$ | 162 556 | 205 030 | −7.10 | −3.86 | $-8.80 \times 10^{-5}$ | $-5.41 \times 10^{-5}$ |
| | 209 851 | | −5.80 | | $-1.00 \times 10^{-4}$ | |
| $5p^34f^36p - 5p^34f^36s$ | 62 513 | 70 252 | −2.10 | −1.60 | $-1.50 \times 10^{-4}$ | $-1.41 \times 10^{-4}$ |
| | 77 209 | | −1.70 | | $-1.80 \times 10^{-4}$ | |
| $5p^34f^36p - 5p^34f^37s$ | 142 597 | 149 861 | −1.89 | −2.49 | $-3.00 \times 10^{-4}$ | $-1.48 \times 10^{-4}$ |
| | 157 545 | | −3.00 | | $-2.50 \times 10^{-4}$ | |

[a] Determined for each SOSA through diagonalization of the Hamiltonian (see sections 2.3 and 2.4).
[b] Determined for each UTA through compact formulae of Bauche *et al* (2015) (see section 2.3).
[c] Evaluated through a least-square fit procedure for each SOSA (see section 2.3).
[d] Evaluated using equation (11) for each UTA (see section 2.3).
[e] Evaluated using equation (10) for each UTA (see section 2.3).

respectively 13 536 304 for the *a posteriori* statistical RTA simulation (without $5p^54f^2$), 14 287 901 for the full HFR calculation with CI (including $5p^54f^2$) and 20 259 942 for the *ab initio* statistical RTA simulation of Sm VIII. Concerning Eu VI, these numbers become 8378 185 (*a posteriori* simulation), 9122 429 (HFR) and 13 029 693 (*ab initio* simulation). Regarding the total line strengths, the results are in good agreement except for two arrays in Sm VIII ($5p^44f^3 - 5p^34f^35d$ and $5p^34f^36p - 5p^34f^35d$) and in Eu VI ($5p^64f^4 - 5p^54f^45d$ and $5p^54f^46p - 5p^54f^45d$) where they differ by a factor of two. These discrepancies are due to the missing weak lines due to the threshold applied to the oscillator strengths in our *a posteriori* RTA simulations.

In tables 5 and 6, we present a comparison between our *a posteriori* and *ab initio* statistical RTA values for the average wavenumber, $\sigma_{av}$, and the correlation parameters $\alpha$ and $\beta$ for each $C_l - C_u$ array in Sm VIII and Eu VI, respectively. Concerning the *a posteriori* RTA simulations, as we use SOSAs, except for the first array of Sm VIII and the fourth one of Eu VI, where UTAs are used instead, there are two or three $\alpha$ and $\beta$ values per E1 transition array considered, depending on if there are two or three resolved SOSA peaks (see, for instance, figure 3 where the distribution of the line strengths of the $5p^34f^36p - 5p^34f^35d$ array in Sm VIII as computed by a full HFR calculation is shown and where one can see that two SOSA peaks are clearly resolved) while for the *ab initio* method, these parameters are calculated using UTAs, i.e. with a single value per E1 array. There are some differences in the $\alpha$ and $\beta$ parameter values, but they are still of the same order of magnitude. These are, along with those in the average wavenumbers, due to the fact that these parameters are least-squares fitted in the *a posteriori* simulations where SOSAs are used while they are calculated exactly by equations (10) and (11) in the *ab initio* simulations where UTAs are employed instead.

In figures 4 and 5, we compare the expansion opacities computed using the atomic data generated by an exact HFR method and by our *a posteriori* and *ab initio* RTA

**Table 6.** Comparison between *a posteriori* and *ab initio* statistical RTA values of the average wavenumber, $\sigma_{av}$, and the correlation parameters $\alpha$ and $\beta$ for each $C_l - C_u$ array in Eu VI.

| | $\sigma_{av}$ ($cm^{-1}$) | | $\alpha$ | | $\beta$ [cm] | |
|---|---|---|---|---|---|---|
| $C_l - C_u$ array | *A posteriori*[a] | *Ab initio*[b] | *A posteriori*[c] | *Ab initio*[d] | *A posteriori*[c] | *Ab initio*[e] |
| $5p^6 4f^4 - 5p^5 4f^4 5d$ | 270 561 | 332 308 | −6.10 | −1.01 | $-3.50 \times 10^{-5}$ | $-6.21 \times 10^{-5}$ |
| | 335 224 | | −3.45 | | $-3.00 \times 10^{-4}$ | |
| $5p^6 4f^4 - 5p^5 4f^4 6s$ | 327 444 | 344 245 | −2.70 | −2.81 | $-9.00 \times 10^{-5}$ | $-4.68 \times 10^{-5}$ |
| | 371 089 | | −2.3 | | $-1.14 \times 10^{-4}$ | |
| $5p^6 4f^4 - 5p^5 4f^4 7s$ | 490 702 | 506 205 | −4.15 | −4.90 | $-1.10 \times 10^{-4}$ | $-4.60 \times 10^{-5}$ |
| | 535 615 | | −4.20 | | $-1.15 \times 10^{-4}$ | |
| $5p^5 4f^5 - 5p^5 4f^4 5d$ | 168 695 | 173 574 | −6.55 | −3.09 | $-5.00 \times 10^{-5}$ | $-6.44 \times 10^{-5}$ |
| $5p^5 4f^4 6p - 5p^5 4f^4 5d$ | 59 261 | 144 941 | −6.70 | −3.76 | $-3.50 \times 10^{-5}$ | $-8.28 \times 10^{-5}$ |
| | 99 735 | | −6.15 | | $-1.30 \times 10^{-4}$ | |
| | 146 319 | | −5.00 | | $-1.30 \times 10^{-4}$ | |
| $5p^5 4f^4 6p - 5p^5 4f^4 6s$ | 52 553 | 59 041 | −0.40 | −0.69 | $-3.00 \times 10^{-4}$ | $-2.15 \times 10^{-4}$ |
| | 63 230 | | −0.75 | | $-1.99 \times 10^{-4}$ | |
| $5p^5 4f^4 6p - 5p^5 4f^4 7s$ | 101 251 | 105 499 | −0.90 | −2.07 | $-2.70 \times 10^{-4}$ | $-2.08 \times 10^{-4}$ |
| | 111 950 | | −4.20 | | $-2.45 \times 10^{-4}$ | |

[a] Determined for each SOSA through diagonalization of the Hamiltonian (see sections 2.3 and 2.4).
[b] Determined for each UTA through compact formulae of Bauche *et al* (2015) (see section 2.3).
[c] Evaluated through a least-square fit procedure for each SOSA (see section 2.3).
[d] Evaluated using equation (11) for each UTA (see section 2.3).
[e] Evaluated using equation (10) for each UTA (see section 2.3).

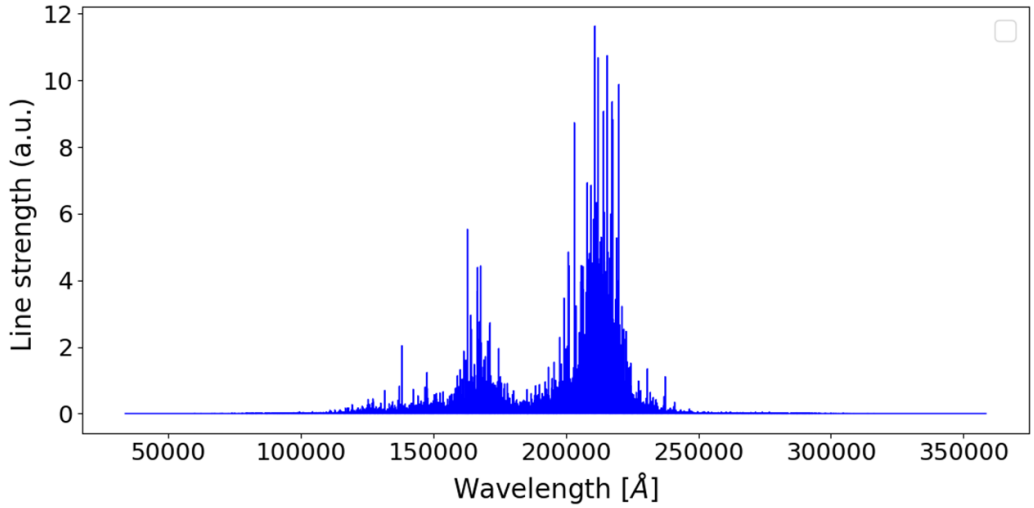


**Figure 3.** Distribution of the line strengths of the $5p^3 4f^3 6p - 5p^3 4f^3 5d$ array in Sm VIII as computed by a full HFR calculation. One can see that two SOSA peaks are clearly resolved.

simulations for early-phase kilonova conditions, namely $\rho = 10^{-10}$ g cm$^{-3}$, $t = 0.1$ day and $T = 50\,000$ K and $T = 38\,000$ K respectively for Sm VIII and Eu VI. These conditions are based on our previous works (Carvajal Gallego *et al* 2022a, 2022b, 2023) where we computed the relative ionic abundances as a function of temperature and allowed us to deduce the temperatures corresponding to the maximum abundance for each of the ions considered in the present study. These correspond to partition functions equal to 951 (*a posteriori* simulation), 1176 (*ab initio* simulation) and 1073 (HFR) in Sm VIII. Concerning Eu VI, the corresponding values were 307 (*a posteriori* simulation), 476 (*ab initio* simulation) and 316 (HFR). In order to see the CI effect on our HFR opacities, which cannot be taken into account in the statistical RTA simulations, we intentionally put to zero all the Slater CI integrals $R^k$ in Cowan's code in order to turn off the CI. As we notice in these figures, the orange curves representing the opacity obtained with the HFR atomic data without CI (all $R^k = 0$), are in satisfactory agreement with the ones obtained with the HFR atomic data with CI. Therefore, the latter, which are not taken into account in the statistical RTA simulations, can be neglected in the expansion opacity computations. Moreover, both statistical RTA simulations (*a posteriori* and *ab initio*) generate similar opacities as the ones computed with the HFR atomic data (with and without CI). The *ab initio* statistical RTA method is therefore an excellent approach to calculate atomic

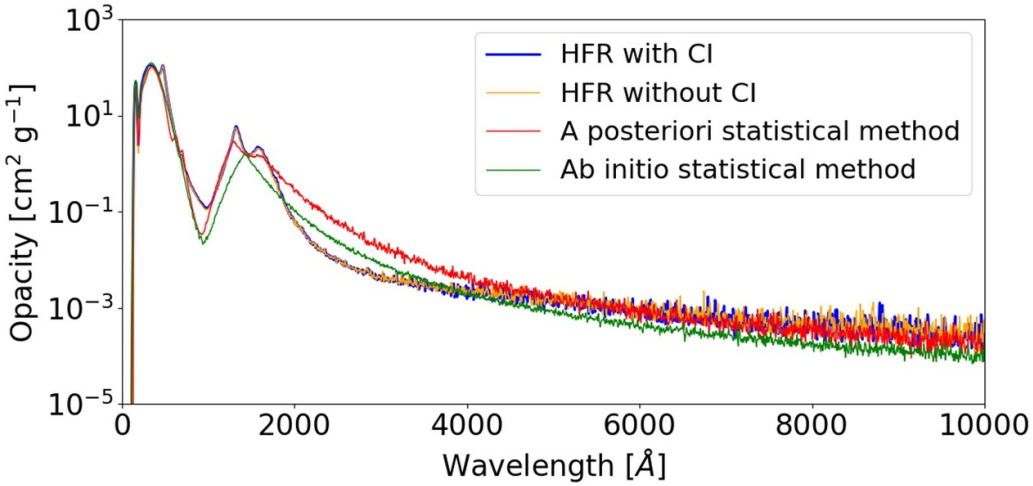


**Figure 4.** Expansion opacities in Sm VIII with $\rho = 10^{-10}$ g cm$^{-3}$, $t = 0.1$ day and $T = 50\,000$ K using the atomic data computed with the HFR method with configuration interaction (CI) (blue curve), without CI (orange curve), simulated with the *a posteriori* statistical RTA method (red curve) and with the *ab initio* statistical RTA method (green curve).

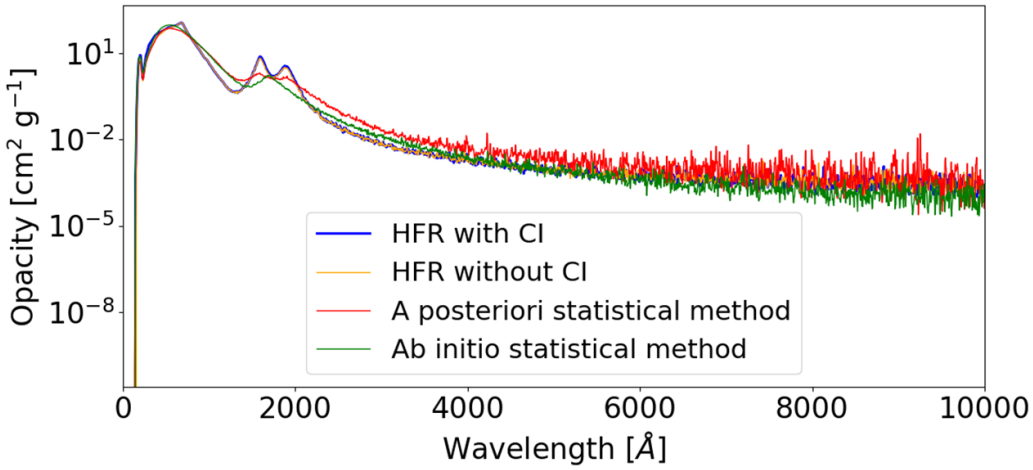


**Figure 5.** Expansion opacities in Eu VI with $\rho = 10^{-10}$ g cm$^{-3}$, $t = 0.1$ day and $T = 38\,000$ K using the atomic data computed with the HFR method with configuration interaction (CI) (blue curve), without CI (orange curve), simulated with the *a posteriori* statistical RTA method (red curve) and with the *ab initio* statistical RTA method (green curve).

data in order to compute expansion opacities for ions where standard computational atomic structure methods such as HFR in Cowan's code are difficult to use through diagonalization.

### 3.3. Dy VIII

Dy VIII is a very complex lanthanide ion characterized by a ground state with a half-filled 4f subshell, namely $5p^4 4f^7$. The matrix of the Hamiltonian, even limited to two configurations (including the ground state and e.g. $5p^3 4f^7 5d$), has an enormous size (60 840 levels), making its diagonalization unfeasible with the current version of Cowan's code. As shown in the previous subsection that the (*ab initio*) statistical RTA simulations reproduced the expansion opacities using the exact atomic data with good agreement, and we can therefore employ this statistical approach for this complex ion with confidence.

The following six configurations have been considered in our statistical RTA simulation in Dy VIII: $5p^4 4f^7$, $5p^3 4f^8$ and $5p^3 4f^7 6p$ in the odd parity and $5p^3 4f^7 5d$, $5p^3 4f^7 6s$ and $5p^3 4f^7 7s$ in the even parity. All the statistical parameters of the different distributions are gathered in table 7 for the configurations and for table 8 for the E1 transition arrays. The total number of levels is equal to 135 135. The issue of matrix size can be easy understood while looking at the huge number of levels per configuration, e.g. about 60 840 levels for $5p^3 4f^7 5d$. The total number of lines generated in Dy VIII reached the enormous number of 1 222 362 566. The $\alpha$ and $\beta$ correlation parameter values with only the average wavenumbers are given in table 9 for each E1 transition array.

The simulated expansion opacity for Dy VIII is shown in figure 6. We have used the same conditions as for Sm VIII, i.e. $T = 50\,000$ K, $\rho = 10^{-10}$ g cm$^{-3}$, $t = 0.1$ day. One can see that the general trend is very similar to the one we observed in both Sm VIII (see figure 4) and Eu VI (see figure 5). Here, however, the Dy VIII opacity reaches a maximum of $4.85 \times 10^3$ cm$^2$ g$^{-1}$ at ∼285 Å.

**Table 7.** Parameters of the statistical distribution of energy levels, $D_C(E)$, i.e. average energy, $E_{av}$, standard deviation, $\sqrt{v_C}$, and total number of levels, $N_C$, for each configuration in Dy VIII as considered in our *ab initio* statistical RTA calculation.

| Configuration | $E^a_{\rm av}$ (cm$^{-1}$) | $\sqrt{v_C}^b$ (cm$^{-1}$) | $N^c_C$ |
|---|---|---|---|
| $5p^4 4f^7$ | 177 349 | 60 217 | 4900 |
| $5p^3 4f^7 5d$ | 487 912 | 86 490 | 60 840 |
| $5p^3 4f^7 6s$ | 615 653 | 75 932 | 12 817 |
| $5p^3 4f^7 7s$ | 850 623 | 76 133 | 12 817 |
| $5p^3 4f^8$ | 244 778 | 59 859 | 5740 |
| $5p^3 4f^7 6p$ | 695 474 | 77 097 | 38 021 |

[a] HFR radial parameter (see section 2.1).
[b] Computed using HFR radial integrals and the compact formulae tabulated in Bauche *et al* (2015) (see section 2.1).
[c] Computed using equation (2) (see section 2.1).

**Table 8.** *Ab initio* statistical RTA values for the number of lines, $L(C_l - C_u)$, the total strength, $S(C_l - C_u)$), and the unweighted, $\sqrt{v_{un}}$, and weighted, $\sqrt{v_w}$, standard deviations of the wavenumber distribution for each $C_l - C_u$ array in Dy VIII.

| $C_l - C_u$ array | $L(C_l - C_u)^a$ | $S(C_l - C_u)^b$ [a.u.] | $\sqrt{v_{un}}^c$ (cm$^{-1}$) | $\sqrt{v_w}^c$ (cm$^{-1}$) |
|---|---|---|---|---|
| $5p^4 4f^7 - 5p^3 4f^7 5d$ | 89 978 658 | 520 824 | 40 198 | 16 451 |
| $5p^4 4f^7 - 5p^3 4f^7 6s$ | 19 512 763 | 24 136 | 33 265 | 16 841 |
| $5p^4 4f^7 - 5p^3 4f^7 7s$ | 19 512 763 | 2855 | 33 128 | 17 110 |
| $5p^3 4f^8 - 5p^3 4f^7 5d$ | 105 556 407 | 140 225 | 49 213 | 16 549 |
| $5p^3 4f^7 6p - 5p^3 4f^3 5d$ | 689 477 967 | 533 565 | 37 459 | 15 388 |
| $5p^3 4f^7 6p - 5p^3 4f^3 6s$ | 149 162 004 | 783 839 | 44 470 | 9977 |
| $5p^3 4f^7 6p - 5p^3 4f^3 7s$ | 149 162 004 | 207 009 | 27 986 | 10 202 |

[a] Calculated using equation (5) (see section 2.2).
[b] Calculated using equation (8) (see section 2.3).
[c] Evaluated using the compact formulae of Bauche-Arnoult *et al* (1979, 1982)(see section 2.3).

**Table 9.** *Ab initio* statistical RTA values of the average wavenumber, $\sigma_{\rm av}$, and the correlation parameters $\alpha$ and $\beta$ for each $C_l - C_u$ array in Dy VIII.

| $C_l - C_u$ array | $\sigma^a_{\rm av}$ (cm$^{-1}$) | $\alpha^b$ | $\beta^c$ (cm) |
|---|---|---|---|
| $5p^4 4f^7 - 5p^3 4f^7 5d$ | 364 652 | −3.80 | $-6.93 \times 10^{-5}$ |
| $5p^4 4f^7 - 5p^3 4f^7 6s$ | 436 759 | −5.96 | $-5.96 \times 10^{-5}$ |
| $5p^4 4f^7 - 5p^3 4f^7 7s$ | 660 745 | −7.77 | $-5.76 \times 10^{-5}$ |
| $5p^3 4f^8 - 5p^3 4f^7 5d$ | 272 138 | −5.04 | $-7.39 \times 10^{-5}$ |
| $5p^3 4f^7 6p - 5p^3 4f^7 5d$ | 201 321 | −5.81 | $-7.39 \times 10^{-5}$ |
| $5p^3 4f^7 6p - 5p^3 4f^7 6s$ | 78 480 | −3.20 | $-1.33 \times 10^{-4}$ |
| $5p^3 4f^7 6p - 5p^3 4f^7 7s$ | 144 861 | −5.09 | $-1.16 \times 10^{-4}$ |

[a] Determined for each UTA through compact formulae of Bauche *et al* (2015) (see section 2.3).
[b] Evaluated using equation (11) for each UTA (see section 2.3).
[c] Evaluated using equation (10) for each UTA (see section 2.3).

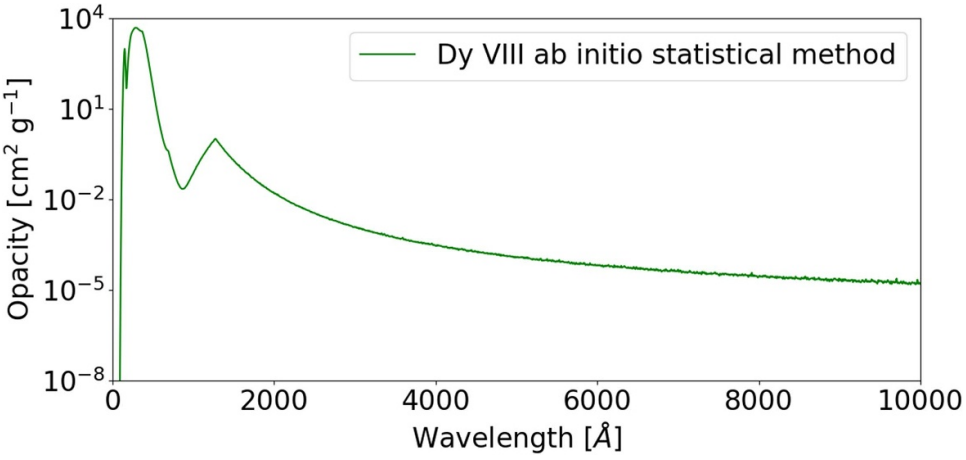


**Figure 6.** Expansion opacities in Dy VIII with $\rho = 10^{-10}$ g cm$^{-3}$, $t = 0.1$ day and $T = 50\,000$ K using the atomic data simulated with the *ab initio* statistical RTA method.

## 4. Conclusions

Atomic data for some complex ions, such as moderately-charged lanthanides, are extremely challenging to calculate with standard atomic structure codes such as the HFR method (Cowan 1981) where a Hamiltonian matrix is built and diagonalized. Therefore, to overcome this issue, it is important to investigate a statistical approach. A considerable advantage of the latter is that there are no limits on the number of configurations introduced to build the model for an ion, whereas using a standard method has limits in that way. In this work, the statistical RTA method of Bauche *et al* (1991, 2015) has been considered and it was demonstrated that, by picking at random the energies of the lower $E_l$ and the upper $E_u$ levels of the atomic transitions, and their corresponding transition amplitudes $a$ in the relevant Gaussian distributions, it is possible to simulate the atomic data and, for the first time, to simulate the corresponding expansion opacities. These statistical RTA simulations allow us to compute reliable astrophysical expansion opacities which are of paramount importance for kilonova light curves and spectral analysis.

## Data availability statement

All data that support the findings of this study are included within the article (and any supplementary files).

## Acknowledgments

H C G is holder of a FRIA fellowship, while P P and P Q are, respectively, Research Associate and Research Director of the Belgian Fund for Scientific Research F.R.S. - FNRS. This project has received funding from the FWO and F.R.S. - FNRS under the Excellence of Science (EOS) Programme (Numbers 0.0228.18 and 0.0004.22). Part of the atomic calculations were made with computational resources provided by the Consortium des Equipements de Calcul Intensif (CECI), funded by the F.R.S. - FNRS Under Grant No. 2.5020.11 and by the Walloon Region of Belgium.

## ORCID iDs

H Carvajal Gallego https://orcid.org/0000-0002-8462-4771
J-C Pain https://orcid.org/0000-0002-7825-1315
M Godefroid https://orcid.org/0000-0003-4192-3875
P Palmeri https://orcid.org/0000-0002-4372-6798
P Quinet https://orcid.org/0000-0002-3937-2640

## References

Abbott B 2017 *Astrophys. J. Lett.* **848** L13
Abbott B *et al* 2017 *Phys. Rev. Lett.* **119** 161101
Banerjee S, Tanaka M, Kato D and Gaigalas G 2023 arXiv:2304.05810v2
Banerjee S, Tanaka M, Kato D, Gaigalas G, Kawaguchi K and Domoto N 2022 *Astrophys. J.* **934** 117
Bar-Shalom A, Klapisch M and Oreg J 2001 *J. Quant. Spectrosc. Radiat. Transfer* **71** 169
Bauche J and Bauche-Arnoult C 1987 *J. Phys. B: At. Mol. Phys.* **20** 1659
Bauche J, Bauche-Arnoult C and Peyrusse O 2015 *Atomic Properties in Hot Plasmas From Levels to Superconfigurations* (Springer)
Bauche J, Bauche-Arnoult C, Wyart J F and Klapisch M 1991 *Phys. Rev.* A **44** 5707
Bauche-Arnoult C, Bauche J and Klapisch M 1979 *Phys. Rev.* A **20** 2424
Bauche-Arnoult C, Bauche J and Klapisch M 1982 *Phys. Rev.* A **25** 2641
Carvajal Gallego H, Berengut J, Palmeri P and Quinet P 2022a *Mon. Not. R. Astron. Soc.* **513** 2302
Carvajal Gallego H, Berengut J, Palmeri P and Quinet P 2022b *Mon. Not. R. Astron. Soc.* **509** 6138
Carvajal Gallego H, Deprince J, Berengut J, Palmeri P and Quinet P 2023 *Mon. Not. R. Astron. Soc.* **518** 332
Carvajal Gallego H, Deprince J, Palmeri P and Quinet P 2023a *Mon. Not. R. Astron. Soc.* **522** 312
Carvajal Gallego H, Deprince J, Palmeri P and Quinet P 2023b *Astron. Astrophys.* submitted
Carvajal Gallego H, Palmeri P and Quinet P 2021 *Mon. Not. R. Astron. Soc.* **501** 1440
Cowan R 1981 *The Theory of Atomic Structure and Spectra* (California University Press)
Deprince J, Carvajal Gallego H, Godefroid M, Goriely S, Palmeri P and Quinet P 2023 *Eur. Phys. J.* D **77** 93
Domoto N, Tanaka M, Kato D, Kawaguchi K, Hotokezaka K and Wanajo S 2022 *Astrophys. J.* **939** 8
Eastman R G and Pinto P A 1993 *Astrophys. J.* **412** 731
Fontes C J, Fryer C L, Hungerford A L, Wollaeger R T and Korobkin O 2020 *Mon. Not. R. Astron. Soc.* **493** 4143
Froese Fischer C, Gaigalas G, Jönsson P and Bieroń J 2019 *Comput. Phys. Commun.* **237** 184
Fujii K and Berengut J C 2020 *Phys. Rev. Lett.* **124** 185002
Gaigalas G, Kato D, Rynkun P, Radžiūtė L and Tanaka M 2019 *Astrophys. J.* S **240** 29
Gaigalas G, Rynkun P, Radžiūtė L, Kato D, Tanaka M and Jönsson P 2020 *Astrophys. J.* S **248** 13
Karazija R 1991 *Sums of Atomic Quantities and Mean Characteristics of Spectra* (Mokslas)
Karazija R and Rudzikaitė L 1988 *Liet. Fiz. Rinkinys* **28** 294
Karp H, Lasher G, Chan K L and Salpeter E E 1977 *Astrophys. J.* **214** 161
Kasen D, Metzger B, Barnes J, Quataert E and Ramirez-Ruiz E 2017 *Nature* **551** 80
Kasen D, Thomas R C and Nugent P 2006 *Astrophys. J.* **651** 266
Moszkowski S A 1962 *Prog. Theor. Phys.* **28** 1
Radžiūtė L, Gaigalas G, Kato D, Rynkun P and Tanaka M 2020 *Astrophys. J.* S **248** 17
Radžiūtė L, Gaigalas G, Kato D, Rynkun P and Tanaka M 2021 *Astrophys. J.* S **257** 29
Rynkun P, Banerjee S, Gaigalas G, Tanaka M, Radzuite L and Kato D 2022 *Astron. Astrophys.* **658** A82
Sobolev V V 1960 *Moving Envelopes of Stars* (Harvard University Press)